3D printing of nanocellulose hydrogel scaffolds with tunable mechanical strength towards wound healing application

Xu, Chunlin; Zhang Molino, Binbin; Wang, Xiaoju; Cheng, Fang; Xu, Wenyang; Molino, Paul; Bacher, Markus; Dandan, Su; Rosenau, Thomas; Willför, Stefan; Wallace, Gordon

Published in:
Journal of Materials Chemistry. B

DOI:
10.1039/c8tb01757c

Published: 01/01/2018

Journal Name

ARTICLE

3D printing of nanocellulose hydrogel scaffolds with tunable mechanical strength towards wound healing application

Received 00th January 20xx,
Accepted 00th January 20xx

DOI: 10.1039/x0xx00000x
www.rsc.org/

Chunlin Xu,*[,a,]† Binbin Zhang Molino,[b,c]† Xiaoju Wang,[a,]† Fang Cheng,*[,d,e] Wenyang, Xu,[a] Paul Molino, [b] Markus Bacher,[f] Dandan Su,[d] Thomas Rosenau,[a,f] Stefan Willför, [a] and Gordon Wallace *[,b]

We present for the first time approaches to 3D-printing of nanocellulose hydrogel scaffolds based on double crosslinking, first by *in situ* Ca^{2+} crosslinking and post-printing by chemical crosslinking with 1,4-butanediol diglycidyl ether (BDDE). Scaffolds were successfully printed from 1% nanocellulose hydrogels, with their mechanical strength being tunable in the range of 3 to 8 kPa. Cell tests suggest that the 3D-printed and BDDE-crosslinked nanocellulose hydrogel scaffolds supported fibroblast cells´ proliferation, which was improving with increasing rigidity. These 3D-printed scaffolds render nanocellulose a new member of the family of promising support structures for crucial cellular processes during wound healing, regeneration and tissue repair.

Introduction

Tissue engineering has become one of the most promising solutions for medical treatments, particularly for healing of chronic wounds. The building blocks of engineered wound healing platforms are usually scaffold materials embodied with cells and mechanical, electrical, or biochemical cues [1, 2]. Both natural and synthetic polymers have been used to mimic the structures of the extracellular matrices (ECM) in native tissues, allowing cells to adhere, proliferate, differentiate, and survive [2-4]. Cells respond differently to those substrates with different stiffness, composition, and structure [5].

Cellulose-based materials have been shown to have great biomedical potential in the construction of ECM-mimicking scaffolds owing to their intrinsic characteristics, such as biocompatibility, lack of cytotoxicity, tunable 3D-architecture and porous microstructures, and desired mechanical properties, although their *in vivo* degradability still remains as a challenge due to lack of the relevant enzyme in the human body [6] Bacterial cellulose is one of those materials that have been intensively studied and developed into commercial applications [7, 8]. However, due to the nature of bacterial cellulose cultivation, post-production shaping remains a challenge for applications, especially in the demanding area of 3D-bioprinting. More recently, also wood-based nanocellulose that is more readily shapeable has been reported to be biocompatible and to be able to support crucial cellular processes during culturing of different cell lines [9, 10]. Earlier findings from our studies suggest that the physical properties of nanocellulose scaffolds have an impact on the cell functions in the matrix [11].

3D-Bioprinting is a process of making a three-dimensional solid object of a specific shape from a digital model with biocompatible 'inks'. It has recently emerged as a technology for fabrication of medical devices. 3D-Printing enables the creation of individual, tailor-made scaffolds to provide desired architectures, and furthermore, integration with biological cues to target cell proliferation in a controlled manner [12-15]. Hydrogels of versatile natural biopolymers, such as gelatin, chitosan, and alginate, have been extensively explored as scaffold materials through the use of bioprinting [16]. Compared with the other biopolymers, nanocelluloses also stand out in the field of bioink formulation serving as platform biomaterial owing to their high mechanical strength as well as the structural similarity mimicking natural ECM. However, the big challenge is to develop printable formulations and to keep the printed scaffolds stable [17]. Markstedt et al. developed an ink of nanocellulose/alginate mixture crosslinkable with Ca^{2+} [18]. However, the alginate hydrogel tends to form loose and unstable structures when placed into a medium in a lower concentration of Ca^{2+}. The same group recently developed inks of nanocellulose/xylan mixtures, with the nanocellulose content being one-third or even less [19]. Though ink formulations can make use of material combinations, using a simple, ideally single-component, ink formulation offers greater promise with regard to printability and stability and possesses more potential in advancing ink properties to better meet the requirements of different applications. To our knowledge, there has been no approach to print biocompatible scaffolds with nanocellulose as the dominant matrix, possessing tunable mechanical properties and stability in the wet state.

The aim of this study was to develop an approach to 3D-printing of nanocellulose hydrogels with double crosslinking. Parameters of printing and geometry design were explored and optimized. The scaffolds were crosslinked during printing by addition of an aqueous Ca^{2+} solution, followed by a post-

[a.] *Johan Gadolin Process Chemistry Centre, Åbo Akademi University, Turku, Finland.*
[b.] *ARC Centre of Excellence for Electromaterials Science, Intelligent Polymer Research Institute, AIIM Faculty, University of Wollongong, Australia.*
[c.] *Faculty of Engineering, Yokohama National University, Japan*
[d.] *School of Pharmaceutical Sciences (Shenzhen), SYSU, China*
[e.] *Cell Biology, Faculty of Science and Engineering, Åbo Akademi University, Turku, Finland.*
[f.] *Division of Chemistry of Renewable Resources, Department of Chemistry, University of Natural Resources and Life Sciences, Vienna, Austria.*

†These authors contributed equally to the manuscript.
*Email: C. Xu, cxu@abo.fi; G. Wallace, gwallace@uow.edu.au
Electronic Supplementary Information (ESI) available: [details of any supplementary information available should be included here]. See DOI: 10.1039/x0xx00000x

printing chemical crosslinking with 1,4-butanediol diglycidyl ether (BDDE). The latter has been proven to be a cytocompatible crosslinking agent that has been widely used in designing crosslinkable hydrogels [20-22]. The rigidity of the printed scaffolds was further tuned by the crosslinking parameters. Biocompatibility and survival, adhesion, and proliferation of human dermal fibroblasts in the printed scaffolds were assessed. Furthermore, the impact of rigidity to scaffolds on cell behavior was investigated.

Experimental

Materials and Methods

A cellulose nanofibril (CNF) hydrogel was prepared from bleached birch kraft pulp as reported [10]. In brief, 100 g of bleached birch kraft pulp was disintegrated in 900 mL of deionized water. 2,2,6,6-Tetramethylpiperidine 1-oxyl (TEMPO) (0.1 mmol/g fiber) and sodium bromide (1.0 mmol/g fiber) were dissolved in deionized water and mixed with the fiber dispersion (0.1 wt%). The pH of the slurry was adjusted to 10.0 by adding 0.5 M NaOH. The oxidation was initiated by adding NaOCl solution (12 wt% active chlorine, 10 mmol/g fiber) dropwise to the slurry. The reaction was kept at pH 10.5 during the reaction by adding 0.5 M NaOH. After 6 h, the mixture was quenched by adding 10 L of ethanol and the pH value of the mixture was adjusted to 7.0 with 1.0 M HCl. The oxidized fibers were thoroughly washed with deionized water to remove the residual chemicals, set to a consistency of 1.0% and homogenized with a Rannie 15 type homogenizer operating at 600 bar and 1000 bar for the first and second pass, respectively. The charge density (carboxylic acid content) of the CNF fibers was determined in dispersion by potentiometric titration [23]. In this study, CNF with charge densities of 1.14 ± 0.07 mmol/g was used.

$CaCl_2$, 1,4-butanediol diglycidyl ether (BDDE), NaOH, and Dulbecco's phosphate buffered saline (with $CaCl_2$ and $MgCl_2$) were purchased from Sigma-Aldrich and used as received.

Human Dermal Fibroblasts (HDF) were purchased from ATCC, Fecal Bovine Serum (FBS) was purchased from Invitrogen, and the MTT kit was purchased from Sigma. The DMEM medium and the antibiotics was made in the in-house medium lab.

3D-Printing

CNF printing and *in situ* crosslinking. CNF printing was carried out on a customized 3D-printer KIMM SPS1000 Bioplotter, consisting of a 3-axis stage movement system, a pneumatic dispensing head and a computer controller. CNF hydrogel was loaded into a 5 cm^3 EFD syringe barrel with a 200 µm precision tip (Nordson Australia & New Zealand), and the syringe was connected to the AD3000C dispensing controller (Iwashita Engineering, Inc.). The dispensing pressure was set to 50 kPa and the printing speed to 500 mm/min. 5% $CaCl_2$ solution was added during printing and the printed scaffolds were stored in in the refrigerator at 4 °C prior to further treatments and tests. Printing patterns were designed using the customized software Bioplot. The printing area was 10 mm x 10 mm, the strut thickness was 200 µm and the strut grid (the space between the centers of the two adjacent struts) was 1 mm. For the lay-down pattern employed in scaffold fabrication, the struts were respectively oriented in three different rotating fashion of 0°/45°/90°/135° (deposition angle of 45°), 0°/60°/120° (deposition angle of 60°), and 0°/90°(deposition angle of 90°), as shown in **Fig. 1**. Also scaffolds with different heights were printed.

Post-print BDDE crosslinking. The printed CNF scaffolds were subjected to further chemical crosslinking by BDDE, the crosslinking protocol being adopted from Kennel et al. 2013 [24]. Scaffolds were washed with deionized water three times and excess water was removed by a pipette. BDDE with a BDDE/cellulose ratio (w/w) of 0.01 and 0.18 (based on anhydroglucose units) for low crosslinking (LC) and high crosslinking (HC) degrees, respectively, was dissolved in 0.25 M NaOH solution and was added into the scaffolds. The reaction took place in an incubator with orbital shaking at 50 °C for two hours. Afterwards, the scaffolds were washed three times with 0.1 M HCl for 15 mins in an orbital shaker, followed by washing with deionized water for three times. The scaffolds were then washed with PBS and kept in PBS prior to other tests.

All NMR spectra were recorded on a Bruker Avance III HD 400 spectrometer (resonance frequency for ^1H 400.13 MHz) equipped with a 4 mm hr-MAS probe head (BBFO) with z–gradients at room temperature with standard Bruker pulse programmes. The samples were swollen in D_2O (99.8 % D). Calibration was done by addition of TMSP-D4 [3-(trimethylsilyl)propionic acid sodium salt D4]. ^1H NMR data were acquired with water suppression using excitation sculpting with gradients and a rotational frequency of 5 kHz.

Analytical Characterization

Optical microscopy. The morphology of the printed scaffolds was assessed with an upright optical microscope coupled with a Toupcam UCMOS 14000KPA camera. Toupview (v. 3.7.2774) software was used to measure the diameter of the printed filaments.

Scanning electron microscopy (SEM). The scaffolds were frozen in liquid nitrogen for 30 min followed by freeze-drying for 72 h under a pressure of 0.7 mbar at -52 °C. The dried scaffolds were sputter-coated with gold. SEM images were taken on a Hitachi S-5500 electron microscope at an acceleration voltage of 5 kV.

Rheology. Studies were carried out on a Physica MCR 301 Rheometer (Anton Paar) with cone-plate geometry (Ø50mm and 1°) at room temperature. Oscillation measurements were performed on the CNF solutions in the LVE range using frequency sweep mode.

Swelling ability. The printed CNF scaffolds were weighed in the wet-state after removing excess water with a pipette. Afterwards, the scaffolds were frozen in liquid nitrogen for 20 min followed by freeze-drying. The freeze-dried scaffolds were weighed, immersed into water and weighed again after 5 min, 30 min, 2 h, 5 h, and 24 h. The water re-sorption ability was calculated as swelling degree:

$$Swelling\ degree = \frac{Weight\ after\ rewetting - Dry\ Weight}{Dry\ Weight}$$

Mechanical tests. The mechanical properties of CNF scaffolds were measured with a Shimadzu EZ-L universal testing machine controlled by the TRAPEZIUMX software. Scaffolds with 4 mm height and different orientation angles were used for this measurement. The compression speed was set to a constant rate of 1.0 mm/min. To simulate the physiological medium, hydrogel scaffolds were kept in PBS (pH 7.4) at least overnight prior to measurement. The Young's modulus was calculated by extrapolating and linear fitting of the elastic region of the stress-

strain curves. The stiffness was calculated from the linear derivative of the stress–strain curve at 5–10% strain. The storage modulus of scaffolds was measured on a Physica MCR 301 Rheometer (Anton Paar) with cone-plate geometry (Ø50mm and 1°) at 25 °C.

Cell assays

Cell culture. Human dermal fibroblast cells (HDF) were maintained in DMEM (4.5 mM glucose) supplemented with 2 mM L-glutamine, 100 IU/mL penicillin and streptomycin and 10% heat-inactivated FBS (Invitrogen) and were incubated at 37 °C with 5% CO_2 and 95% humidity. Cell culturing on 2D-plates and various CNF 3D-matrices with thicknesses of 2 or 3 mm was carried out using HDF cells for *in vitro* assessment of the common cellular functions (cell attachment, viability, and proliferation on scaffolds). Cells were seeded onto the CNF matrix by dropping on the film or aerogel surface at a seed density of 1×10^5 cells per sample in a 24-well plate.

Quantitative cell viability MTT assay and cell attachment assay. Cytotoxicity evaluation of 3D CNF scaffolds was performed after 24 h of cell incubation using the MTT kit (Sigma) according to the manufacturer's manual. After staining, the plates were immediately read out at 570 nm using a microplate reader. To detect maintained adherence of cells on the 3D matrix, cell suspensions were kept in contact with the matrix for 12 h and non-adherent cells were washed off. The plate was frozen for 30 min at −70 °C. The plate was then thawed, and cells were stained in 0.5% crystal violet dye for 20 min. After washing, samples were fixed with methanol for 20 min, and then read out at 570 nm.

Cell proliferation assay and confocal imaging of cells on the scaffold. For *in vitro* proliferation assays, cells samples were fixed after 72 h post incubation with 3.7% paraformaldehyde for 30 min and a mixture of acetone and methanol (1:1) for 5 min in ice. Triton X (0.2%) in PBS was used to permeabilize the cell membranes, and Triton X (10%) in FBS was used for blocking for 2 h. The cells were stained with Phalloidin conjugated with Alexa Fluor 488 for 3 h, and counterstained with DAPI blue for 3 min before mounting on glass slides. Confocal images were acquired at room temperature using Zeiss Zen software on a Zeiss LSM780 confocal laser scanning microscope (Carl Zeiss, Inc.) with Plan-Apochromat 10x. The fluorochromes Alexa Fluor 488 and 405 were used.

Statistical analysis. The results are expressed as the mean ± STD. Comparisons between two groups were analyzed by two-tailed t tests. Comparisons between multiple groups were analyzed by 1-way ANOVA test. $p<0.05$ was considered significant. Statistical differences were calculated with the two-tailed unpaired t-test and differences were considered significant at $p\leq0.05$.

Results and discussion

Printing of CNF hydrogel

Ascribed to its shear-thinning behavior, a CNF hydrogel can be extruded at high shear rate and layered to scaffolds. The rheological behavior of the formulation is critical to satisfying printing needs. As shown in **Fig. 2**, CNF hydrogels of both 0.72 wt% and 1.0 wt% showed typical gelling properties with storage modulus being much higher than loss modulus at low angular frequency, and elastic modulus starting to decrease at high angular frequency and further became lower than crossed loss modulus. This is in agreement with previously reported rheological properties of CNF hydrogel [25]. The frequency at cross point reflects the required lowest pressure for printing, and also the mechanical strength of the printed hydrogel. 1.0 wt% CNF formed a more stable gel that remained on the bottom of the sample vial in comparison to 0.72 wt% CNF, cf. the images in **Fig. 2**. Hydrogels of both concentrations were suitable for printing, the setup pressure range for 1.0 wt% CNF (48 kPa or above) being significantly higher than that for 0.72 wt% CNF (about 19 kPa). Printed 1.0 wt% CNF scaffolds maintained their shapes in fridge over three months while those from 0.72% CNF tended to lose their structure with time, for example after 24 hours storage as shown by cf. the images in **Fig. 2**.

In order to print scaffolds with tunable mechanical strength, a dual-crosslinking strategy was applied (**Fig. 1a**). Concentrated $CaCl_2$ solution was added onto the printed scaffolds during printing to strengthen the structure by Coulomb (ionic) interactions, the bivalent Ca^{2+} cations crosslinking two carboxylate groups on the CNF matrix which had been introduced before by TEMPO-mediated cellulose oxidation. Afterwards, as post-print modification, crosslinking by BDDE of different dosages was applied. This was done to further increase the strength of the printed scaffolds. This BDDE crosslinking approach has been well established for crosslinking of polysaccharides and has been confirmed to be biocompatible. It has been widely used to crosslink hydrogels under mild conditions [26] and was analogously applied to the printed and pre-linked CNF material in our study. A reaction time of up to 2 h was applied for the BDDE modification, but this can be shortened to about 30 min if necessary. BDDE crosslinking of printed CNF hydrogels was confirmed by ^{1}H NMR (**Fig. S1**). After crosslinking at low-level, a small peak at 1.5-1.6 ppm appeared, which intensified in the NMR spectra of more highly crosslinked scaffolds. This is in a good agreement with the reported chemical shifts of the BDDE molecule ($-CH_2-CH_2-$) in the crosslinking of other polysaccharides [24, 27, 28].

Mechanical properties of the printed scaffolds

The compressive Young's modulus was significantly increased after the BDDE treatment (**Fig. 3a**), which is yet another reliable proof of crosslinking. We also designed three lay-down patterns with the adjacent strut angle varied in fashion of 0°/90°, 0°/60°/120°, and 0°/45°/90°/135°. It has been reported that the position and orientation of the extruded struts in lay-down pattern affect the scaffold mechanical properties in a broad and complex manner. [29, 30]. Notably, the pore shapes vary in quadrangular, triangular, and complex polygonal geometries for these printed scaffolds as the deposition angle varied from 90° and 60° to 45°. Among these hydrogel scaffolds, the architecture at 0°/90° imposed a higher mechanical modulus than the other two catalogues. Similar observation was also reported in 3D printed scaffolds of poly(ε-carprolactone) with respect to the same variation of lay-down pattern by Domingos et al. [31] It was claimed that the decrease in the amplitude of the deposition angle implied a larger fused contact area, which would lead to a decrease of the compressive stress experienced locally. It was also speculated that the adjacent struts were more prone to slide from each other and cause the deformation of the scaffold. Thus, the CNF scaffolds with 90° pattern were focused on in the later studies.

The scaffolds with high-level crosslinking had a modulus of 7.44 kPa, which is almost double of that of scaffolds without crosslinking (i.e. 3.45 kPa). Compressive Young's moduli of scaffolds printed with CNF as single component have not been reported before. In a few recent studies [17-19], the mechanical strength of CNF scaffolds prepared by 3D-printing was studied in the form of either dried scaffolds or cast disks. In our opinion, the mechanical properties of CNF scaffolds in their wet state are more critical for understanding how it can affect the cell behavior.

ECM scaffolds possess well-defined elastic moduli ranging from 10 Pa for very soft tissues such as fat to 10 kPa for muscles, and even higher for hard tissues, such as bones [32]. With regard to wound healing applications, studies showed that the substrate stiffness affects the interaction between NIH-3T3 fibroblast cells and the matrix. Scaffolds with a modulus of 3 kPa were stiff enough for cells to start spreading, and this cell spreading maximized on substrates with moduli of about 10 kPa [33]. Another study revealed that fibroblasts may reside in the substrates and adapt to the mechanical environment by altering their stiffness to match the substrate's stiffness, though always remaining slightly softer [33]. However, these fibroblast cells failed to match substrate stiffness in tissues harder than 10 kPa. The Young's moduli measured for our printed CNF scaffolds ranged from 3 kPa to 8 kPa depending on the crosslinking level, and lower than 3 kPa for the scaffolds with 60° orientation. Therefore, they are well suitable for applications of skin wound healing.

Moreover, skin tissues take not only compressive but also shear forces from the surrounding environment [35, 36]. Therefore, the hydrogel formation was further characterized, with G' being higher than G'' over the entire frequency range (**Fig. 3b**). The G' value was determined to reach 10 kPa depending on the applied frequency, resulting in a self-supported and free-standing hydrogel up to the millimeter scale.

Structural stability

To evaluate the stability of the printed scaffolds, the scaffold matured in the Ca^{2+} aqueous solution was firmly squeezed by wafer tweezers (**Fig. 4**). The outstanding elasticity of the material allowed it to recover immediately after pressure release in all directions. As shown by the stress-strain curve in **Fig. 3c**, all printed scaffolds sustained a strain of 50% upon compression without failure. Initial linear correlation of elasticity was observed for 20% of strain or higher. The high rigidity of the scaffolds is ascribed to the strong hydrogen bonding and the Ca^{2+}/carboxylate crosslinking, which also plays a significant role in crosslinking of polysaccharide hydrogels with high carboxylate content, such as alginate [18, 37].

SEM images show the topological and cross-sectional view of the printed scaffolds after freeze-drying. The difference between scaffolds before and after BDDE crosslinking is clearly illustrated in **Fig. 4**. Porous structures are observed on the strut surface of scaffolds after crosslinking by BDDE. The scaffold with higher crosslinking level possesses higher microporosity compared to the less crosslinked ones. The tentative explanation is that chemical crosslinking by BDDE increases the rigidity of the hydrogel and thus the hydrogel tends to maintain its structure better while drying, also depicted in other studies where cellulose aerogel was prepared from crosslinking of cellulose hydrogel [38].

The printed hydrogel scaffolds were stored in PBS medium for up to three months and kept their structure according to visual observation. The strut size of printed scaffolds was estimated from optical microscopy images (**Fig. S2**). By fitting squared lines to the edge of struts, the size of all scaffolds including original and crosslinked ones showed only negligible variation. This indicates that BDDE crosslinking and Coulomb interactions contribute to the stability of scaffolds.

Water re-sorption

Water retention stability of ECM is critical in regulating cellular activities [39]. Nanocellulose hydrogel surfaces are highly hydrophilic. Ca^{2+} crosslinked (no BDDE), low-level BDDE crosslinked, and high-level BDDE crosslinked hydrogels before drying had swelling degrees of 277.7±4.1, 307.1±22.1, and 212.1±19.4, respectively (**Fig. 5**). These materials were freeze-dried and then soaked in water for re-swelling. All scaffolds resorbed water immediately after being re-immersed, demonstrating high water uptake ability. The Ca^{2+} crosslinked scaffold was able to uptake water 100 times relative to its own weight, similar to the low-level BDDE crosslinked scaffolds The high-level BDDE crosslinked matrix resorbed less water, but still possessed a swelling degree of around 70. Thus, the high water uptake ability was not impaired by chemical crosslinking.

It is worth pointing out that the scaffolds were able to maintain their shapes after drying and after resorbing water. An earlier study reported that nanocellulose hydrogel prepared by TEMPO-mediated oxidation tended to collapse after drying [17]. However, our scaffolds maintained good structural stability, which is ascribed to the combination of ionic Ca^{2+} and covalent BDDE crosslinking. This is also in line with observation by SEM images, which showed that dried scaffolds particularly with the high-level BDDE crosslinking were able to keep their microporous structure (**Fig. 4**).

3D CNF scaffolds supported survival, adhesion, and proliferation of human fibroblasts

We next assessed the biocompatibility of the 3D-printed CNF scaffolds, a key feature for any ECM-mimicking matrix. Cell survival on 3D-CNF scaffolds was tested with human dermal fibroblasts (HDF) isolated from human foreskin, a key cell component involved in wound healing. After 24 hours of cell incubation within the CNF matrix, cell samples were examined according to the MTT colorimetric assay to quantitatively measure the capability of viable cells to metabolize the dye 3-(4,5-dimethylthiazol-2-yl)-2,5-diphenyltetrazolium bromide. The 3D-CNF scaffolds demonstrated great HDF cell viability compared with the control 2D cell culture (**Fig. 6a**).

Fibroblast cells are critical in the wound healing process. They are involved in secreting ECM and interacting with the local microenvironment 40. Fibroblast cell lines are well established to test natural or synthetic scaffolds that are developed for wound healing applications. In our previous studies, the hydrogels originating from the same TEMPO-oxidized CNF showed good biocompatibility with epithelially derived Hela cells, hematopoietic Jurkat cells, and mouse fibroblasts [10, 11, 41].

Next, the cell adhesion capability was measured after 12 hours of cell incubation into/onto the CNF scaffolds according to the crystal violet assay. In comparison with 2D control samples, cells adhered slightly less on the 3D printing matrix (**Fig. 7**). The matrix thickness influenced cell adhesion, with 3 mm samples having a higher percentage of cell attachment (84-86.5%) than

2 mm samples (78.25-79.25%)(**Fig. 6b**), which would be due to an effect of the larger surface areas of the former for cells to adhere.

Moreover, 3D-CNF materials support cell proliferation after longer incubation periods. After three days post cell seeding, there are 2-4 times more HDF cells on 3D CNF samples as compared to 2D control coverslip samples (**Fig. 7**). Scaffolds with 15 layers (3 mm) supported cell proliferation to a greater extent than those with 11 layers (2 mm). It is known that the 3D-geometry of the tissue-like scaffolds is critical for cells to bridge gaps and to fill the voids to proliferate [42,43]. As 3 mm samples induce more cell proliferation than 2 mm samples, enhanced cell proliferation might be the consequence of larger spatial areas and more appropriate geometries available to hold cells. Interestingly, among the 3D samples, cells in the HC matrix were growing faster than in LC matrix, whereas LC matrix induced more cell growth than non-crosslinked matrix, suggesting the positive role of crosslinking in supporting cell proliferation (**Fig. 7**).

A clear trend to increase cell proliferation was observed for scaffolds that were non-BDDE crosslinked (ctrl, 3 mm) to BDDE crosslinked at low level (LC, 3 mm) and further to high BDDE crosslinked level (HC, 3 mm) (**Fig. 7a**). Their Young's moduli at compression mode were 3.45 kPa, 4.52 kPa, and 7.44 kPa, respectively. This is highly in line with the above observation that the NIH-3T3 fibroblast cell-matrix interaction responds to matrix stiffness: a scaffold of a modulus of 3 kPa is stiff enough for cells to start spreading, with cell spread being maximized on the substrate with a modulus of about 10 kPa [33]. Scaffolds with higher stiffness than our current maximum value could be interesting, but will require different crosslinking approaches, which could tune the stiffness over a wider range towards higher values. One also needs to keep in mind that fibroblast cells might not adapt to ECM matrix with too high stiffness [34]**:** 10 kPa was shown to be that limit for fibroblast cells in some studies.

In summary, the good biocompatibility and only a marginal inhibition of cell adhesion provide good opportunities for the safe application of these materials in wound healing therapies.

Conclusions

We have developed an approach to tailor hydrogel scaffolds by 3D-printing of 1 wt% one-component-only TEMPO-oxidized nanocellulose hydrogel, for the first time. The printed scaffolds were able to maintain their structural integrity through *in situ* crosslinking by Ca^{2+} cations, and their stability was further enhanced by post-print covalent BDDE crosslinking. This way, the mechanical strength of the scaffolds could be well tuned in the range of 3 to 8 kPa.

Cell tests confirmed that the fabricated scaffolds are non-toxic to fibroblast cells. Compared with 2D structures, 3D printing strengthens the capability of the generated matrix in promoting cell proliferation, which is critical in producing a prompt wound healing. The rigidity of the scaffolds has a clear impact on cell proliferation - cell proliferation is promoted when the rigidity is increased within the tunable range of 3 – 8 kPa. This correlation is, for the first time, demonstrated by 3D-printed nanocellulose hydrogels.

We are quite positive that 3D-printing nanocellulose materials will become an important tool in future wound healing, skin regeneration and tissue repair approaches.

Conflicts of interest

There are no conflicts to declare.

Acknowledgements

Xu C. and Wang X. would like to thank Academy of Finland for financial support to the research and scientific mobility (project number: 268455; 298325). This work is also part of the activities within the Johan Gadolin Process Chemistry Centre, the Centre of Excellence established by Åbo Akademi University during 2015-2018. B. Z. Molino, P. Molino, and G. G. Wallace would like to thank the Australian National Fabrication Facility (materials node) for equipment use, and the Australian Research Council for funding through the ARC Centre of Excellence for Electromaterials Science (CE140100012).

Notes and references

1 C. Sahlgren, A. Meinander, H. Zhang, F. Cheng, M. Preis, C. Xu, and T. A. Salminen, et al.., *Advanced Healthcare Materials,* 2017, **6**, 1700258.
2 B. M. Baker, B. Trappmann, W. Y. Wang, M. S. Sakar, I. L. Lim, V. B. Shenoy, J. A. Burdick and C. S. Chen, *Nature Materials,* 2015, **14**, 1262.
3 L. Moroni, J. de Wijn and C. van Blitterswijk, *Biomaterials,* 2006, **27**, 974.
4 M. W. Tibbitt and K. S. Anseth, *Journal of Biotechnology,* 2015, **193**, 66.
5 D. E. Discher, P. Janmey and Y.-l. Wang, *Science*, 2005, **310**, 1139.
6 N. B. Shelke, R. James, C. T. Laurencin and S. G. Kumbar, *Polymers for Advanced Technologies,* 2014, **25**, 448.
7 W. Czaja, D. Young, M. Kawecki and R. Brown, *Biomacromolecules,* 2007, **8**, 1.
8 D. Wanna, C. Alama, D. Toivola and P. Alam, *Advances in Natural Sciences: Nanoscience and Nanotechnology,* 2013, **4**, 4.
9 Y.-R. Lou, L. Kanninen, T. Kuisma, J. Niklander, L. A. Noon, D. Burks, A. Urtti and Y. Marjo, *Stem Cells and Development,* 2014, **23**, 380.
10 J. Liu, F. Cheng, H. Grénman, S. Spoljaric, J. Seppälä, J. E. Eriksson, S. Willför and C. Xu, *Carbohydrate Polymers,* 2016, **148**, 259.
11 J. Liu, G. Chinga-Carrasco, F. Cheng, W. Xu, S. Willför, K. Syverud and C. Xu, *Cellulose,* 2016, **23**, 3129.
12 N. Sandler, I. Salmela, A. Fallarero, A. Rosling, M. Khajeheian, R. Kolakovic, N. Genina, J. Nyman and P. Vuorela, *International Journal of Pharmaceutics.,* 2014, **459**, 62.
13 S. Murphy and A. Atala, *Nature Biotechnology,* 2014, **32**, 773.
14 W. Xu, X. Wang, N. Sandler, S. Willför and C. Xu, *ACS Sustainable Chemistry & Engineering,* 2018, **6**, 5663.
15 W. Xu, A. Pranovich, C. Xu and et al. *Carbohydrate Polymers,* 2018, **187**, 51.
16 S. Murphy, A. Atala, *Nature Biotechnology ,* 2014, **32**, 773.

17 K. M. Håkansson, I. C. Henriksson, C. de la Peña Vázquez, V. Kuzmenko, K. Markstedt, P. Enoksson and G. Paul, *Advanced Materials Technologies,* 2016, **1**, 1600096.
18 K. Markstedt, A. Mantas, I. Tournier, H. Martinez Avila, D. Haegg and P. Gatenholm, *Biomacromolecules,* 2015, **16**, 1489.
19 K. Markstedt, A. Escalante, G. Toriz and P. Gatenholm, *ACS Applied Materials & Interfaces,* 2017, **9**, 40878.
20 C. E. Schanté, G. Zuber, C. Herlin and T. F. Vandamme, *Carbohydrate Polymers,* 2011, **85**, 469.
21 R. Yang, L. Tan, L. Cen and Z. Zhang, *RSC Advances,* 2016, **6**, 16838.
22 X. Li, W. Xue, Y. Liu, D. Fan, C. Zhu and X. Ma, *Journal of Materials Chemistry B,* 2015, **3**, 4742.
23 G. Chinga-Carrasco and K. Syverud, *Journal of Biomaterials Applications,* 2014, **29**, 423.
24 L. Kenne, S. Gohil, E. M. Nilsson, A. Karlsson, D. Ericsson, A. H. Kenne and L. I. Nord, *Carbohydrate Polymers,* 2013, **91**, 410.
25 T. Moberg, K. Sahlin, K. Yao, S. Geng, G. Westman, Q. Zhou, K. Oksman and M. Rigdahl, *Cellulose,* 2017, **24**, 2499.
26 K. De Boulle, R. Glogau, T. Kono, M. Nathan, A. Tezel, J.-X. Roca-Martinez, S. Paliwal and D. Stroumpoulis, *Dermatologic Surgery,* 2013, **39**, 1758.
27 B. Yang, X. Guo, H. Zang and J. Liu, *Carbohydrate Polymers,* 2015, **131**, 233.
28 F. J. Wende, S. Gohil, L. I. Nord, A. H. Kenne and C. Sandström, *Carbohydrate Polymers,* 2017, **157**, 1525.
29 L. Moroni, J. de Wijn and C. van Blitterswijk, *Biomaterials,* 2006, **27**, 974.
30 A. D. Olubamiji, Z. Izadifar, J. L. Si, D. M. Cooper, B. F. Eames and D. X. Chen, *Biofabrication,* 2016, **8**, 025020.
31 M. Domingos, F. Intranuovo, T. Russo, R. De Santis, A. Gloria, L. Ambrosio, J. Ciurana and P. Bartolo, *Biofabrication,* 2013, **5**, 045004.
32 I. Levental, P. C. Georges and P. A. Janmey, *Soft Matter,* 2007, **3**, 299.
33 T. Yeung, P. C. Georges, L. A. Flanagan, B. Marg, M. Ortiz, M. Funaki, N. Zahir, W. Ming, V. Weaver and P. A. Janmey, *Cell Motil Cytoskeleton,* 2005, **60**, 24.
34 J. Solon, I. Levental, K. Sengupta, P. C. Georges and P. A. Janmey, *Biophysical Journal,* 2007, **93**, 4453.
35 J. Zhao, M. Griffin, J. Cai, S. Li, P. E. Bulter and D. M. Kalaskar, *Biochemical Engineering Journal,* 2016, **109**, 268.
36 B. Pei, W. Wang, Y. Fan, X. Wang, F. Watari and X. Li, *Regenerative Biomaterials,* 2017, **4**, 257.
37 J. Liao, B. Wang, Y. Huang, Y. Qu, J. Peng and Z. Qian, *ACS Omega,* 2017, **2**, 443.
38 H. Liu, A. Wang, X. Xu, M. Wang, S. Shang, S. Liu and J. Song, *RSC Advances,* 2016, **6**, 42854.
39 J. H. Jeong, Y. Liang, M. Jang, C. Cha, C. Chu, H. Lee, W. Jung, J. W. Kim, S. A. Boppart and H. Kong, *TISSUE ENGINEERING: Part A,* 2013, **19**, 1275.
40 P. Bainbridge, *J Wound Care,* 2013, **22**, 407.
41 A. Rashad, K. Mustafa, E. B. Heggse and K. Syverud, *Biomacromolecules ,* 2017, **18**, 1238.
42 E. Knight and S. Przyborski, *Journal of Anatomy,* 2015, **227**, 746.
43 S. Shin, S. Park, M. Park, E. Jeong, K. Na, H. J. Youn and J. Hyun, *BioResources,* 2017, **12**, 2941.

Journal Name

ARTICLE

Figure 1. Illustration of 3D printing of CNF hydrogels: a) schematic illustration of printing process and the two-step crosslinking strategy; b) printing patterns, top view of 45°, 60°, and 90° patterns and 3D-view of the 90° scaffold model.

Figure 2. Rheology of CNF hydrogels with different concentrations (0.72 wt% and 1.0 wt%). Inserted images: the two hydrogel solutions in 3 ml vials put upside down; printed scaffolds illustrating a stable structure in the case of the 1.0 wt% hydrogel and an unstable product in the case of the 0.72 wt% hydrogel.

Figure 3. Mechanical properties of printed double-crosslinked scaffolds: a) compressive Young's modulus, b) stress-strain curve, and c) shear modulus of 90° scaffolds.

Figure 4. Printed scaffold (90°) toughness by pins pressing (a-f); SEM images of printed scaffolds (90°): (g-i) cross-section, (j-l) surface morphology. LC and HC indicate low and high BDDE crosslinking degree, respectively.

Figure 5. Water absorption as a function of time for freeze-dried scaffolds (90°) without BDDE and with low and high levels of BDDE crosslinking. The swelling degree was calculated according to Eq. 1.

Figure. 6. HDF cells cultured on printed CNF scaffolds: a) cell survival rate after 24 h of incubation (MTT assay); b) cell adhesion after 12 h of incubation (crystal violet assay). Bar = mean ± STD, n = 4.

Figure 7. HDF cells cultured on printed CNF scaffolds: (a) cell proliferation and (b) confocal images after 3 days of incubation. Scale bar: 200 µm. Bar = mean ± STD, n=4. * $p < 0.1$; ** $p < 0.01$; *** $p < 0.001$.

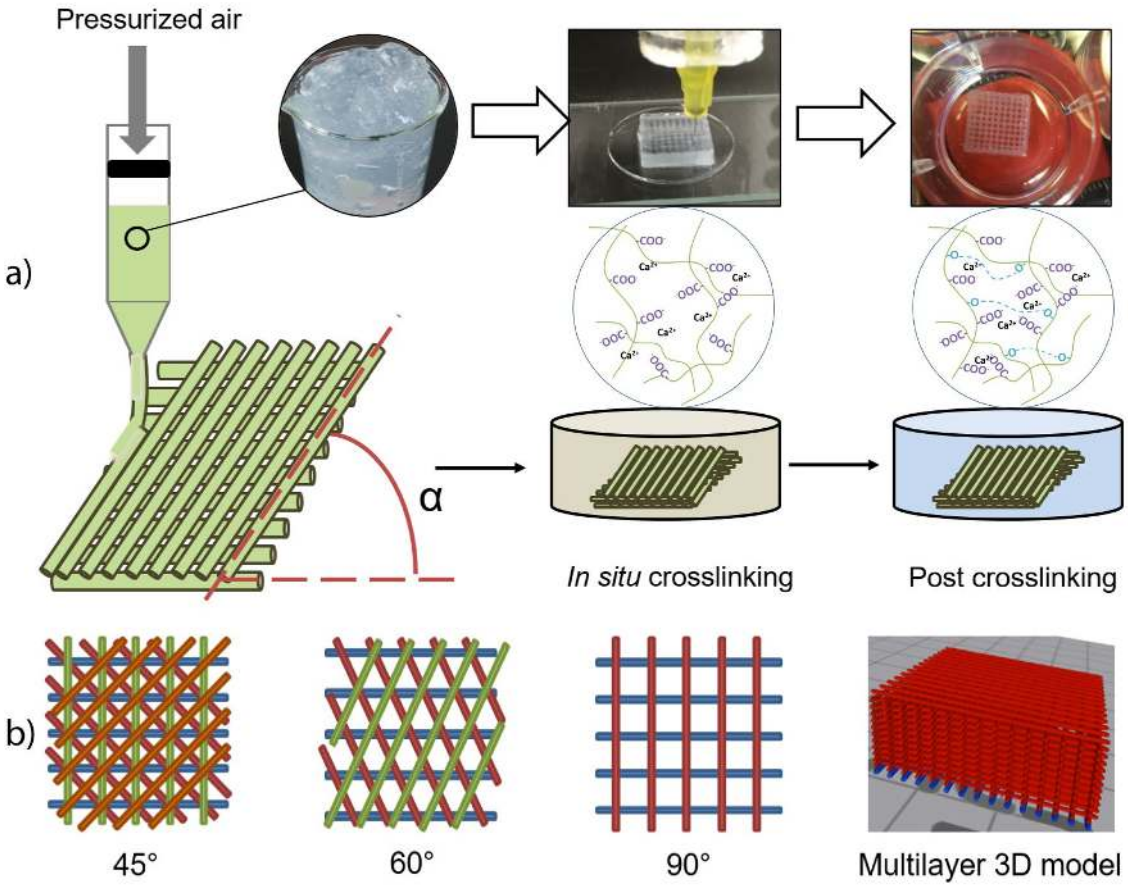

Figure 1.

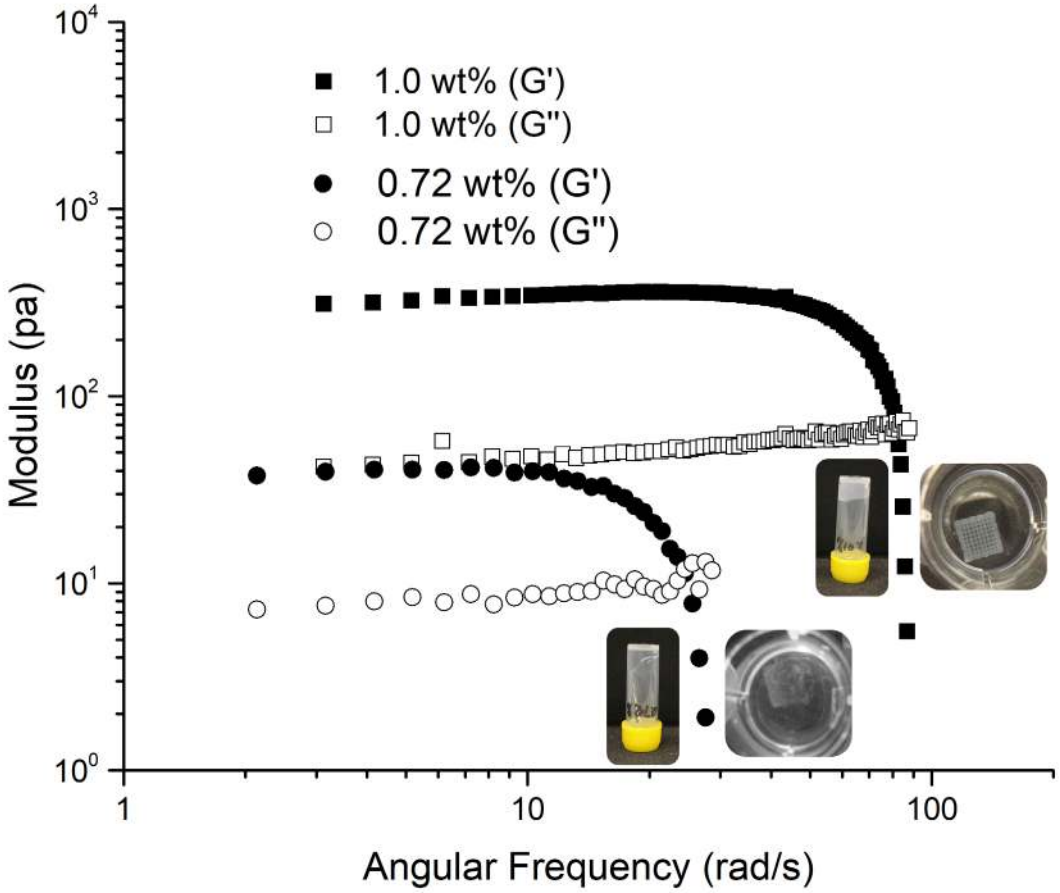
1.0 wt% (G')
1.0 wt% (G")
0.72 wt% (G')
0.72 wt% (G")
Modulus (pa)
Angular Frequency (rad/s)
10^4
10^3
10^2
10^1
10^0
1
10
100

Figure 2.

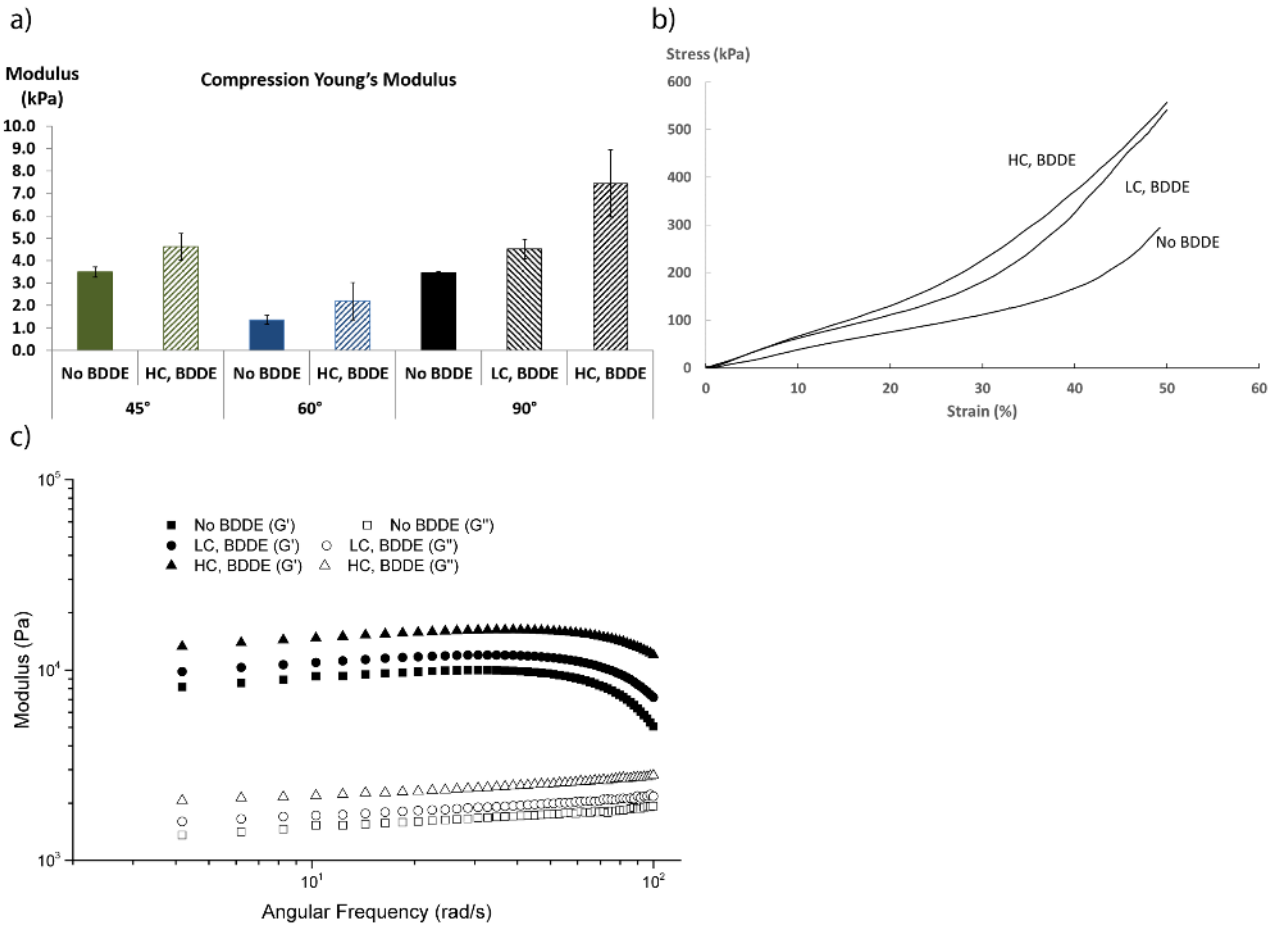

Figure 3.

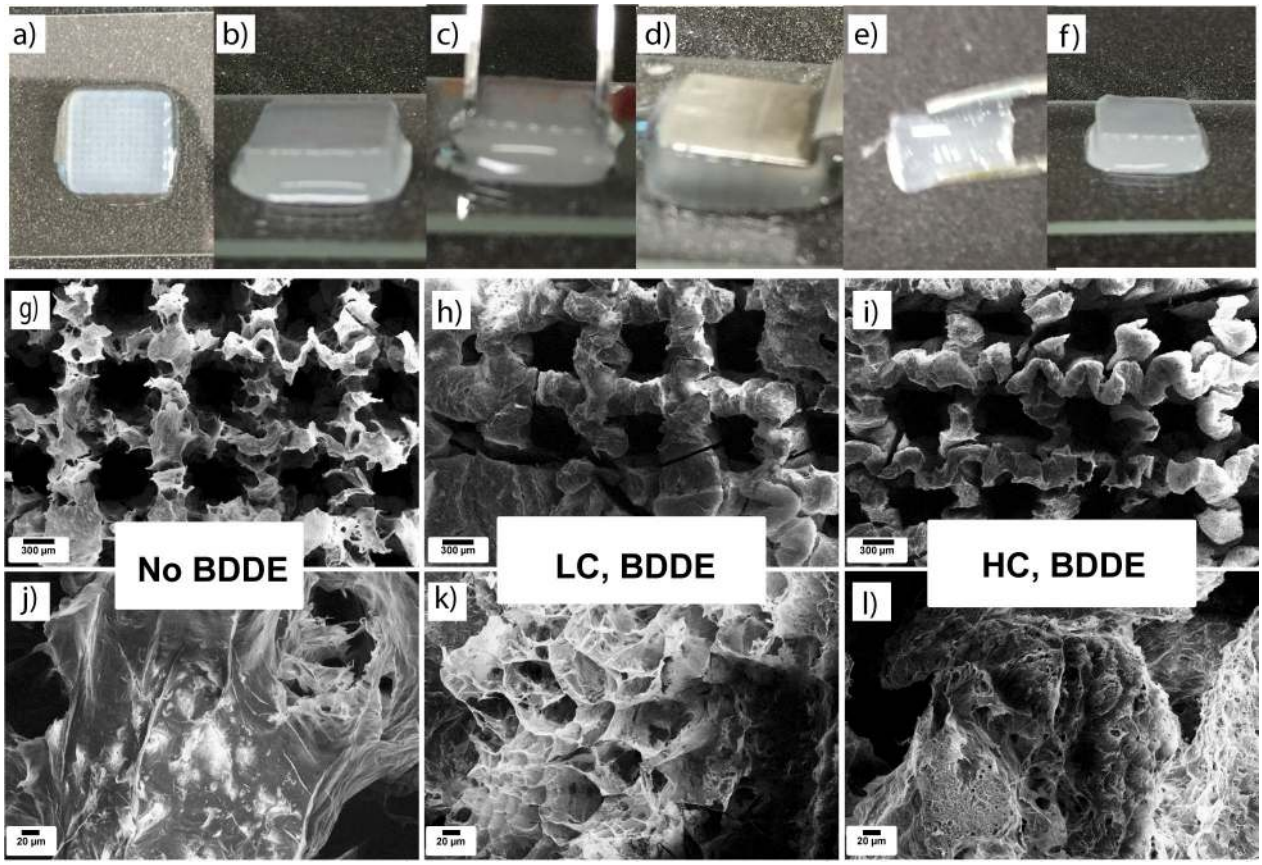

Figure 4.

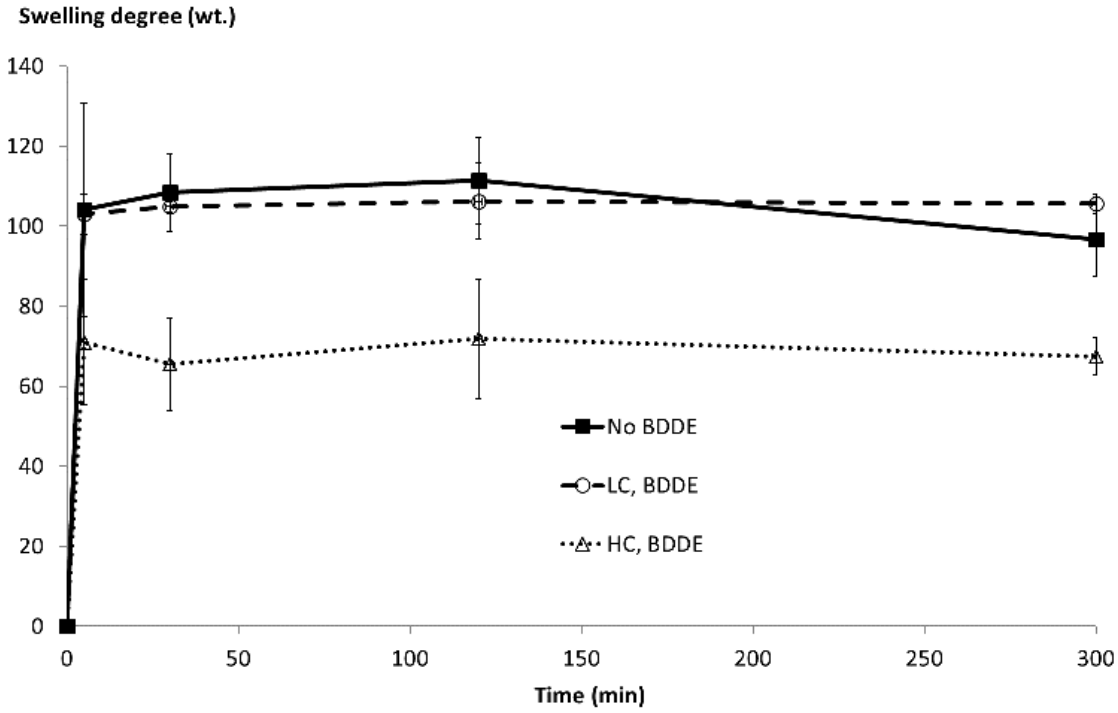

Figure 5.

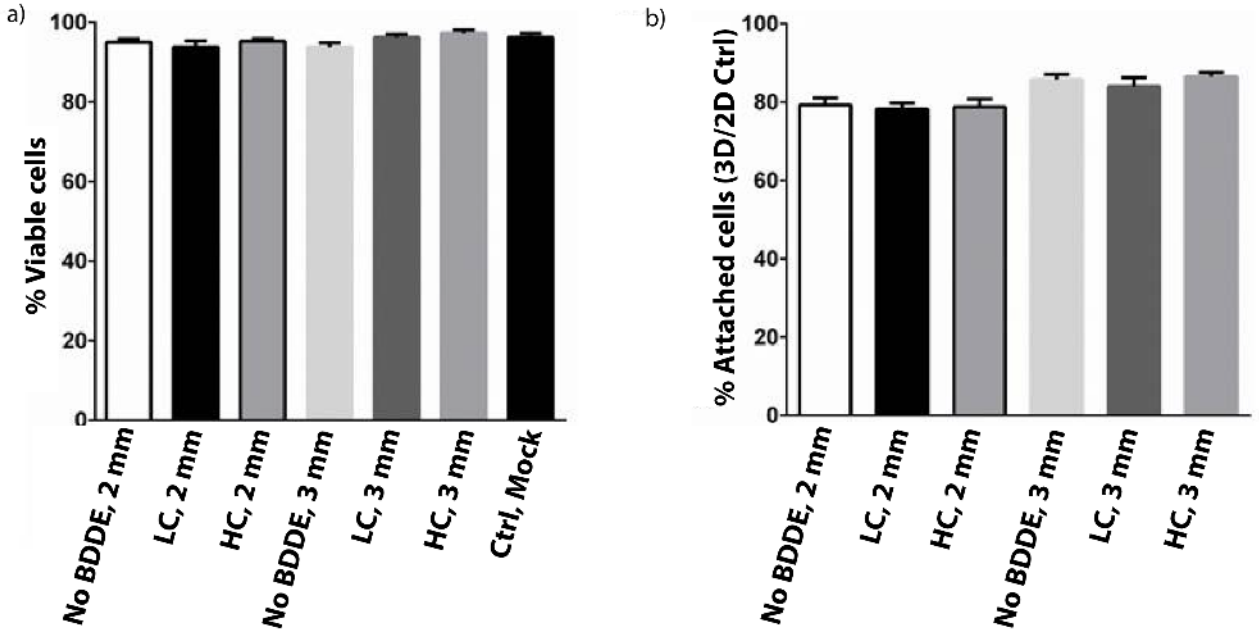

Figure. 6.

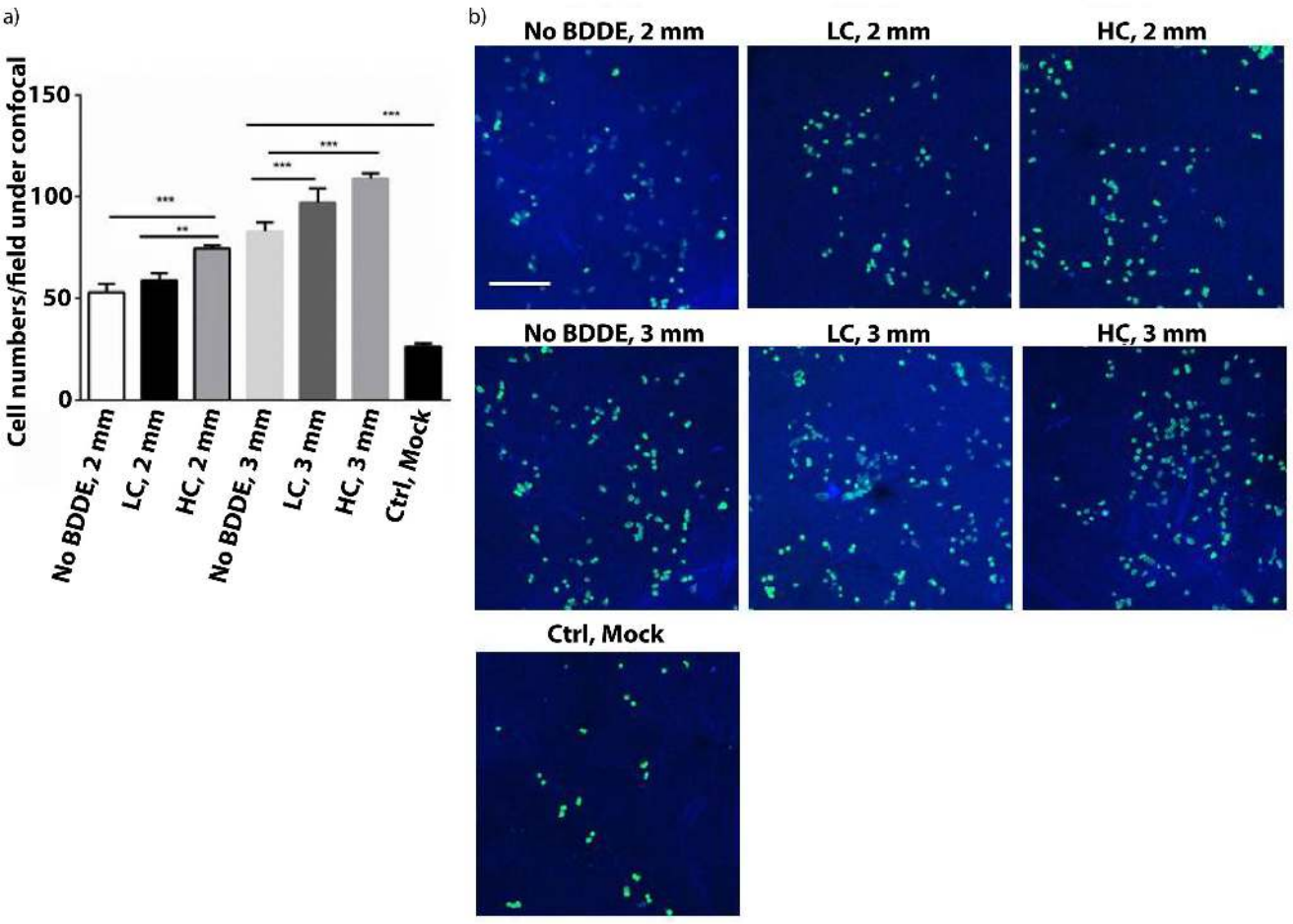

Figure 7.